A Simulative Analysis of the Performance of IEEE 802.11p and ARIB STD-T109

Julian Heinovski, Florian Klingler, Falko Dressler, Christoph Sommer*

Heinz Nixdorf Institute and Dept. of Computer Science
Paderborn University, Germany

Abstract

Vehicular networking, formerly a theorized application of wireless networking concepts to the road, is already seeing first deployments. As a consequence, the focus of research and development is shifting to higher layer aspects, that is, investigating the performance of systems from an application layer perspective. It is important to remember, though, that these applications rest on wholly different networking stacks, depending on whether they are being deployed in the U.S., in Europe, or in Japan. To ensure that simulative performance studies, the tool of choice for many researchers, are valid for more than one region, a differentiated view on (and a means of comparing) network performance across networking stacks is needed. To remedy this, we conducted an extensive simulation study which compares the performance of IEEE 802.11p and ARIB T109. Other than earlier studies, we take into account both their differences on the physical layer (5.9 GHz vs. 700 MHz band) as well as in medium access (pure CSMA/CA vs. a combination with TDMA). We base our results on an Open Source implementation of the ARIB T109 standard we developed for the vehicular network simulation framework Veins, validating results against an analytical study. Our model also encompasses parameters for a computationally inexpensive shadow fading model for suburban environments, the result of an extensive measurement campaign.

1. Introduction

We are currently seeing first deployments of vehicular networking around the world. With this, what used to be a purely theoretical application of wireless networking concepts to the road has become a reality: Japanese automakers are selling first car models that include Intelligent Transportation System (ITS) functionality, the U.S. government has announced plans to make ITS mandatory [1], and developments in Europe indicate similar plans.

With this, the attention of research and development has been shifting to higher layer aspects of communication systems. Instead of lower layer studies, whole applications are studied in large deployments. Such large-scale studies are made possible by computer simulation, which has quickly become the tool of choice for many researchers [2].

For such computer simulations, it is crucial that detailed and realistic models of lower layer effects (e.g., medium access and signal propagation) that are specific to the region of deployment are employed: The U.S. and Europe standards are based on WLAN in OCB mode operating in the 5.9 GHz frequency band (IEEE Std 802.11p [3], see Section 3 in this manuscript), which relies on CSMA/CA to coordinate multiple access. Japan uses the same physical layer in the 700 MHz frequency band, but employs an adapted medium access layer that mixes CSMA/CA with time slotted access (ARIB STD-T109 [4], see Section 4 in this manuscript).

The results of this divide are twofold: First, protocols in the different regions have to cope with very different physical propagation characteristics, most prominently in terms of path loss and shadow fading (owing to the different frequency). Second, channel characteristics in these regions also vary in terms of delay and capacity (owing to the different medium access scheme). However, existing Open Source tools for computer simulation offer physical and medium access models for only either one, but not both of the standards, limiting comparability. Studies have, so far, only focused on protocol performance in either of the regions, limiting the comparability of systems, but also raising the question to what degree a protocol developed for one region can be operated in another region – and what its performance might be.

We therefore present a first comparison of system performance taking into account the different medium access and physical layer properties of the channel in the U.S. and Europe as well as in Japan. This allows us to point out individual benefits and drawbacks. The basis of this comparison is an Open Source implementation of the Japanese ARIB T109 stack for the vehicular network simulation framework Veins [5], which we make publicly available. We also report on the results of an analytical performance study

*Corresponding author
Email addresses: julian.heinovski@ccs-labs.org (Julian Heinovski), klingler@ccs-labs.org (Florian Klingler), dressler@ccs-labs.org (Falko Dressler), sommer@ccs-labs.org (Christoph Sommer)

Article published in Elsevier Computer Communications 122 (2018) 84-92. (10.1016/j.comcom.2018.03.016)

we used for validation. As our physical layer model also captures shadow fading effects by buildings in suburban areas, we also conducted (and report on) a measurement campaign to parameterize the model for operation in the 700 MHz frequency band.

This manuscript constitutes an extended version of our previous work [6], now also including a differentiated view on the effects of physical layer vs. medium access and an analytical study complementing the simulation study.

Our contributions can be summarized as follows:

- We perform extensive simulation studies that compare the performance of the U.S./European IEEE 802.11p and Japanese ARIB T109 standards in a realistic setting, pointing out their individual benefits and drawbacks.
- Our results are based on an implementation of the ARIB T109 standard for the vehicular network simulation framework Veins, which we make available as Open Source.[1] It includes realistic models of both the unique medium access and physical layer characteristics of ARIB T109.
- We detail results of the measurement campaign used to parameterize the model of shadow fading by buildings in suburban areas for the 700 MHz band.
- We compare simulation results to upper and lower bounds of used metrics achieved from an analytical study of the performance of ARIB T109.

2. Related Work

There is a substantial body of work on physical layer properties of the 700 MHz band. One of the first channel characterization studies for 700 MHz in the context of vehicular communication for both LOS and NLOS scenarios was conducted by Sevlian et al. [7]. They conclude that many of the assumptions that hold true for IEEE 802.11p in 5.9 GHz do not transfer well to the 700 MHz band. This serves as further motivation for our work. Later, Fernandez et al. [8] investigated path loss for both 5.9 GHz and 700 MHz in LOS and NLOS conditions. They present parameters for a simple model that uses different path loss coefficients depending on the overall scenario and presence of LOS. The observed values are in line with similar works from the literature. In a later paper [9] they further correlate the used antenna height to adapted path loss coefficients in a freespace scenario. They show that the antenna height has no significant impact on the path loss of 700 MHz. Still later [10], the authors examine the path loss characteristics of convoy traffic in the 5.9 GHz and 700 MHz bands. In each of these studies, however, modelling higher layer effects was not in the scope of work.

Looking at the 700 MHz band from a communication protocols perspective, Minato et al. [11] combine message dissemination on the 5.9 GHz and 700 MHz band. They deploy relay stations near intersections which receive frames transmitted by vehicles in the 700 MHz band, and relay the frames using the 5.9 GHz band. With their approach the authors can increase the frame reception rate compared to using only a single frequency band. However, their simulations are conducted without an adapted medium access model for ARIB T109 as well as with the ITU-R P. 1411-1 [12] path loss model, which only contains shadow fading coefficients for 5.2 GHz.

Sai et al. [13] compare NLOS communication in the 5.9 GHz and 700 MHz band for urban environments using intersection collision avoidance as an application example. In essence they show that with 700 MHz the communication distance and overall packet delivery ratio in NLOS scenarios is higher than on 5.9 GHz. Yet, they use a proprietary network simulator and do not reveal details of their medium access model. Further, the work is based on the ITU-R P. 1411-6 [14] path loss model which (like the above mentioned standard) only contains obstacle shadow fading parameters for 5.2 GHz. More recently, Abunei et al. [15] studied the impact of buildings on the communication of 5.9 GHz and 700 MHz from an application point of view. They conclude that communication on 700 MHz is much less affected by building shadowing, and thus recommend it as back-up for vehicular communication. Their simulation model uses building obstacle shadowing according to the model proposed by Sommer et al. [16], however they are using the same set of parameters for both frequency bands. Moreover their investigation did not consider medium access characteristics of ARIB T109.

Yokomori et al. [17] instead focused their efforts on the medium access layer, studying the benefit of a decentralized TDMA system versus the pure CSMA/CA part of ARIB T109 and, later [18], the benefit of frame reordering. On the lower layers, however, an abstract physical layer model (e.g., radio transmissions cannot penetrate matter) is employed.

Summing up, vehicular communication at 700 MHz has, to date, been predominantly investigated only *(a)* at the physical layer (abstracting away from higher layer protocols) or *(b)* only at higher layers (abstracting away from medium access and/or physical layer characteristics). Our work fills this gap by providing an investigation of vehicular communication that combines accurate modeling of ARIB T109 medium access with realistic propagation models for 700 MHz in urban areas.

3. IEEE 802.11p

The IEEE 802.11p standard [3] is an amendment to the IEEE 802.11 WLAN standard written to support Inter-Vehicle Communication (IVC) and Roadside-to-Vehicle Communication (RVC). It was created for vehicular communications, since these have different characteristics than

[1] `http://veins.car2x.org/`

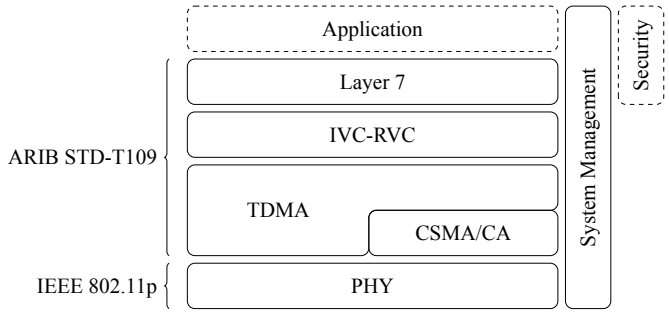

Figure 1: The protocol stack of ARIB STD-T109. Dashed lines indicate entities which are out of the scope of the standard.

usual wireless communications, for example short connection times. It extends the Orthogonal Frequency Division Multiplexing (OFDM) physical layer (from IEEE 802.11a [19]) to operation in the 5.9 GHz band. Most importantly, it also introduces a novel operation mode, called Outside the Context of a BSS (OCB) mode, which allows nodes to operate without being part of a Basic Service Set (BSS). Instead of a lengthy join procedure to establish parameters like modulation and coding scheme, the node uses well-known parameters for accessing the channel. Building upon this standard, later the IEEE 1609 WAVE family of standards was designed to represent a complete ITS stack in the U.S. [20]. Similarly, in Europe, the ETSI ITS-G5 family of standards [21] builds on IEEE 802.11p as an access layer for vehicles and Roadside Units (RSUs) to provide IVC and RVC.

For accessing the radio channel the access layers build on IEEE 802.11p and inherit the CSMA/CA mechanism of IEEE 802.11: A node performs Clear Channel Assessment (CCA) before accessing the channel, that is, it tries to detect whether the channel is free (based on detecting an ongoing transmission or a certain minimum power on the channel); if unsuccessful (channel sensed *busy*), it enters a backoff state and tries again later.

4. ARIB STD-T109

In parallel to the developments in the U.S. and Europe, the Japanese research and standardization organization for radio telecommunication and broadcasting developed ARIB STD-T109 [4], a standard for operating ITS in the 700 MHz band. One of the major goals was to reduce the number of traffic accidents by informing vehicles and their drivers about current traffic conditions and other vehicles in the near field.

Figure 1 shows its protocol stack, which contains:

1. a physical layer based on IEEE 802.11p,
2. a medium access layer (MAC), which realizes a combination of TDMA and CSMA/CA channel access,
3. an *IVC-RVC Layer*, which maintains channel access parameters, maintains clock synchronization, and handles communication control,
4. *Layer 7*, which represents an interface for communicating with end-user applications and dealing with security.

ARIB T109 specifies wireless communication using a physical layer very similar to IEEE 802.11p, but operating on a center frequency of 760 MHz. In contrast to IEEE 802.11p, however, its medium access layer makes a much clearer distinction between the following two classes of traffic: IVC (traffic between vehicles, called *mobile stations*) and RVC (traffic sent to vehicles from RSUs, called *base stations*). For this, ARIB T109 employs a TDMA medium access scheme on top of CSMA/CA. Medium access is therefore subject to two carrier sense functions:

- A *virtual* carrier sense function which utilizes a basic TDMA scheme in every node.
- A *physical* carrier sense function which additionally utilizes a CSMA/CA scheme in mobile stations.

For the TDMA scheme, time is divided into long control cycles of 100 000 µs each, an example of which is shown in Figure 2. Each of these is split into 16 smaller cycles starting at integer multiples of 6240 µs (thus, the last period is 160 µs longer than the preceding 15 cycles). The actual TDMA scheme happens within those short cycles, each of which is flexibly divided into two periods. The period from 0 µs until at most 3024 µs is called *RVC period* and represents time where no vehicles are allowed to access the channel. The reasoning for this prioritization is that, since the base stations are connected to several sensors deployed along the roads [13], they have more knowledge about the current situation and therefore deserve a higher priority for distributing safety information.

Each base station can be assigned an arbitrary subperiod within each RVC period (called its *transmission period* in the standard), during which it (and only it) is allowed to access the channel. Using another medium access scheme (such as CSMA/CA) is not needed, as it is assumed that subperiods are well-configured in base stations to avoid concurrent channel access by RSUs in physical proximity.

The remaining time in each cycle (after the RVC period) represents time where vehicles are allowed to compete for access to the channel. For this, they use a physical carrier sense function (i.e., CSMA/CA) to avoid concurrent channel access with other mobile stations. Vehicles learn about RVC periods in each of the 16 cycles from information embedded in the header of each frame. This information is disseminated in a multi-hop fashion, originating from RSUs and propagating until a hop limit is reached.

Time synchronization among nodes is achieved via *over-the-air* synchronization. Frame headers include the current local time at the sender, which mobile stations use to adjust their local clocks (compensated for processing delays). RSUs synchronize their clocks – preferably from an external time source like GPS; optionally, they can rely on the same mechanism as mobile nodes (but will only trust other RSUs to provide accurate enough values).

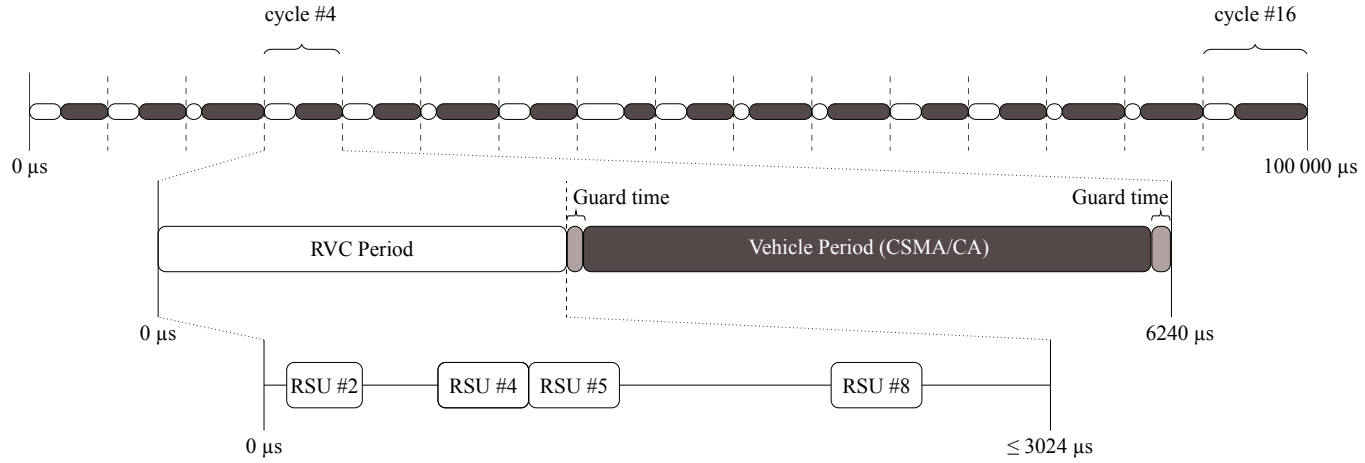

Figure 2: The 100 000 µs control cycle for transmission control which is split into 16 smaller cycles. Those cycles are again divided into two periods by the TDMA scheme. The RVC period is further subdivided into subperiods for individual RSUs.

5. Radio Propagation Model

Since protocols' coping with different shadow fading characteristics of 5.9 GHz and 760 MHz is at the heart of performance studies, these characteristics need to be represented in computer simulations.

Packet level simulations commonly derive the success probability of an incoming transmission from its Signal to Interference and Noise Ratio (SINR). For this, the received power P_r of a signal is commonly calculated using the simple link budget equation

$$P_r[\text{dBm}] = P_t[\text{dBm}] + G_t[\text{dB}] + G_r[\text{dB}] - \sum L_x[\text{dB}], \quad (1)$$

where P_t denotes the transmit power, $G_{t,r}$ are the antenna gains, and individual terms L_x model attenuation due to path loss, slow fading, and fast fading.

Without loss of generality, we assume that a packet level simulation calculates the pure Line of Sight (LOS) path loss component L_{path} using the simple Friis model [22]

$$L_{\text{path}}[\text{dB}] = 10 \log_{10} \left(\left(4\pi \frac{d}{\lambda} \right)^2 \right), \quad (2)$$

where λ is the wave length of the radio transmission and d is the distance between sender and receiver. Further, as in the following we measure and calculate the mean received power over a large number of samples, we disregard the fast fading component of loss in the following considerations.

Most importantly, though, to account for Non Line of Sight (NLOS) characteristics, we need to consider a loss term L_{obs} which models shadow fading due to static obstacles.

5.1. Base Model

We base our model on the shadow fading model described by Sommer et al. [16], which calculates

$$L_{\text{obs}}[\text{dB}] = \beta n + \gamma d_{\text{m}}, \quad (3)$$

where n is the number of exterior walls of an obstacle intersected by the direct line of sight between sender and receiver, d_m is the sum total of distances between each pair of intersection points bordering an obstacle, and β and γ are empirically determined. This allows the model to capture loss effects more complex than a simple yes/no decision (whether two nodes are in LOS), making it particularly suitable for simulations of non-regular building geometries such as those encountered in suburban parts of cities. Summing up, while this model still abstracts away from microscopic effects such as reflections, it can provide a computationally inexpensive approximation of macroscopic effects that is suitable for medium to large scale simulations.

Commonly used values for β and γ for shadowing effects of a building on IEEE 802.11p transmissions at 5.9 GHz are in the range of $\beta = 9\,\text{dB}$ per wall and $\gamma = 0.4\,\text{dB/m}$.

5.2. Model Fitting

Naturally, known values for the 5.9 GHz band will not apply to transmissions in the 700 MHz band, as reported by Fernandez et al. [8]. Their measurement campaign yields way different path loss coefficients for both frequencies in LOS as well as NLOS environments. Thus, in order to adjust the obstacle model to the 700 MHz frequency, we conducted experiments measuring the influence of buildings in a suburban area on the signal. Our measurement area was comprised of several roads and intersections in a suburban part of Paderborn, Germany. Figure 3a depicts a typical straight stretch of road in this part of the city, Figure 3b depicts a typical intersection, both with typical buildings.

Table 1 gives a brief overview of the experiment design: We used omnidirectional antennas to minimize the influence of the cars' orientation. We used two SDRs to transmit simple bursts of power, each set to a fixed center frequency. Measurements with 5.9 GHz were conducted for validating

Environment	mix of roads in suburban area
Radio frontend	Ettus USRP N210 (2 TX, 2 RX)
Frequency	868 MHz and 5.9 GHz
GPS Receivers	2x u-blox NEO-7N
GPS logging interval	every 500 ms
Antennas	roof-mounted omnidirectional
Sample size	100×10^3 samples (over multiple hours)

Table 1: Parameters of the measurement campaign.

results against the existing model parameters. For the other SDR we chose 868 MHz since it is available for civil use while still being reasonably close to the target frequency of 760 MHz. Two more SDRs logged the signal strength at the receiving side. Two GPS receivers, also equipped with roof-mounted antennas, logged the cars' position.

In total, we collected 100×10^3 samples over the course of multiple hours. After fitting the data to the model in Equation (3), we arrive at computed model parameters of $\beta = 0.1\,\text{dB}$ per wall and $\gamma = 0.4\,\text{dB/m}$. As expected, these model parameters reflect the effect that lower-frequency transmissions are affected less by building shadowing.

Figure 4a contains a particularly illustrative excerpt of the larger measurement campaign. Here, the sending car is parked next to the street. The receiving car passes the sender and rounds two corners, disappearing behind buildings. The total length of the trajectory is approx. 130 m, with linear distances between sender and receiver between 3 m and approx. 48 m. The excerpt is thus comprised of segments with direct line of sight between sender and receiver, segments with one, and segments with multiple buildings obstructing the line of sight. Of special interest is a point on the receiver trajectory, marked *point A*, where a small line of sight corridor between two buildings exists.

Figure 4b illustrates the measurement results gathered on this example trajectory of our measurement campaign, along with the results of model fitting of Equation (3) to all measurement results. As can be seen, measurement

(a) Typical straight stretch of road.

(b) Typical road intersection.

Figure 3: Experiments in a suburban area. The near car uses SDRs to transmit at 5.9 GHz and 868 MHz. Another car logs received signal strength at both frequencies.

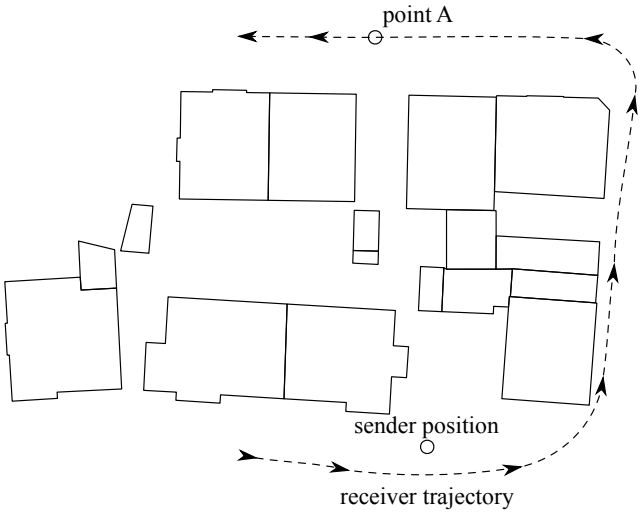

(a) Positions of buildings relative to the position of the sender and the trajectory of the receiver in an example setting of the measurement campaign. At *point A* a small LOS corridor leads to an increased signal strength.

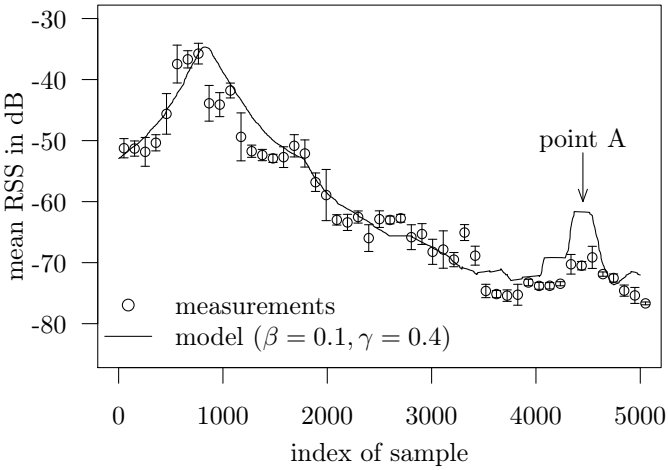

(b) Fit between the analytical model and the mean received signal strength at 868 MHz as well as 1.5 times the standard deviation, measured at points in the example setting shown. At point A we see the increased mean signal strength due to the LOS corridor.

Figure 4: One of the settings examined in our measurement campaign in a suburban part of Paderborn, Germany.

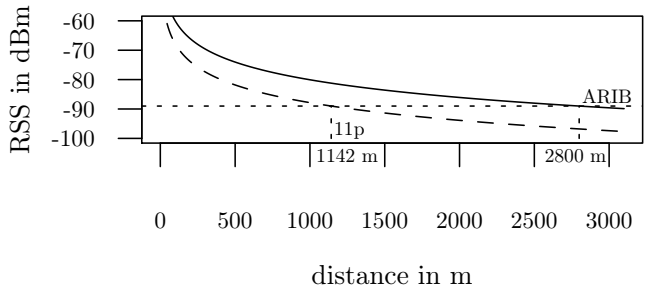

Figure 5: Communication distance limits using a freespace path loss model and a transmit power of 20 dBm (100 mW) for IEEE 802.11p (5.89 GHz), and 10 dBm (10 mW) for ARIB STD-T109 (760 MHz); the horizontal line denotes the assumed receiver sensitivity of −89 dBm, which determines the maximum communication range.

data and model are closely aligned on a macroscopic scale: As the distance between sender and receiver first decreases then increases, the received signal strength (RSS, given in dB relative to the maximum measured) first climbs then falls off, as predicted by Equation (2). When the receiver rounds the first corner and disappears behind the first building (approx. at the time sample 1750 is recorded), the received signal strength drops; and it keeps dropping as more buildings get between sender and receiver. It is also apparent that the macroscopic model is unable to capture two effects on a finer scale: First, none of the quick oscillations are captured by the slow fading model, as can be expected. Second, the line of sight corridor at *point A* is overestimated, as the model ignores the impact of partly (obstructed) Fresnel zones and only focuses on the line of sight. Overall, though, the computed model parameters of $\beta = 0.1\,\text{dB}$ per wall and $\gamma = 0.4\,\text{dB/m}$ can be seen to allow Equation (3) to closely model the real world measurements.

6. Analytical evaluation of ARIB STD-T109

In the following we assume an OFDM PHY with 10 MHz bandwidth as specified in the current version of IEEE 802.11 [23] and used in the ARIB T109 standard [4].

6.1. Distance bounds

First we evaluate the maximum communication distance for wireless data transmissions according to IEEE 802.11p [23] and ARIB T109 [4]. For simplicity we assume a freespace path loss model and a communication range only limited by the sensitivity of the wireless card in the receiver. Further, no antenna gains are assumed. The received signal strength is derived according to Equations (1) and (2).

In Figure 5 we show the received signal strength over distance when transmitting with a power of 20 dBm on 5.89 GHz for IEEE 802.11p, and a power of 10 dBm for ARIB T109, as well as the theoretical upper bound of communication distance for an assumed receiver sensitivity of −89 dBm: 1142 m for IEEE 802.11p, 2800 m for ARIB T109.

6.2. Delay bounds

For the calculation of delay bounds, we set all timing parameters according to the standard. In brief,

$$\begin{aligned} T_{\text{preamble}} &= 32\,\mu\text{s} \\ T_{\text{signal}} = T_{\text{sym}} &= 8\,\mu\text{s} \\ t_{\text{SIFS}} &= 32\,\mu\text{s} \\ t_{\text{DIFS}} &= t_{\text{SIFS}} + 2 \times t_{\text{slot-CSMA}} = 58\,\mu\text{s} \\ t_{\text{slot-CSMA}} &= 13\,\mu\text{s} \\ t_{\text{tick-TDMA}} &= 16\,\mu\text{s} \\ \text{CW} &= 63 \text{ slots.} \end{aligned}$$

Further we assume an application payload of 100 Byte, as well as 22 Byte IVC/RVC header, 8 Byte LLC header, 24 Byte MAC control field, and 4 Byte frame check sequence. This yields a total of $l = 1264$ bit payload.

When transmitting this payload at a bitrate of 6 Mbit/s (thus $N_{\text{DBPS}} = 48$ bit per symbol), the time $t_{\text{tx-1264}}$ for doing so can be calculated as

$$\begin{aligned} t_{\text{tx-1264}} &= T_{\text{preamble}} + T_{\text{signal}} + T_{\text{sym}} \times \left\lceil \tfrac{16+l+6}{N_{\text{DBPS}}} \right\rceil \\ &= 32\,\mu\text{s} + 8\,\mu\text{s} + 8\,\mu\text{s} \times \left\lceil \tfrac{16+1264+6}{48} \right\rceil \\ &= 256\,\mu\text{s}. \end{aligned} \tag{4}$$

As ARIB T109 employs a TDMA scheme we want to explore the limits for channel access, hence the lower and upper bound of time it takes from the application handing down the contents of a frame to the MAC, up until the point the frame was transmitted. For this we assume an empty channel and empty MAC queues. To recap, each control cycle has a length of 100 000 µs, consisting of sixteen cycles having a length of: $t_{\text{cycle15}} = 6240\,\mu\text{s}$ for the first fifteen cycles of a 100 000 µs control cycle and $t_{\text{cycle16}} = 6400\,\mu\text{s}$ for the last cycle. Every cycle contains one RVC period of up to 3024 µs, and one vehicle period consisting of the rest of the time of this cycle. For each vehicle period, an additional guard time of at least (and by default) $t_{\text{guard}} = 4 \times t_{\text{tick-TDMA}} = 64\,\mu\text{s}$ at the beginning and end of the vehicle period is added. Further each RVC period can contain one subperiod for each configured RSU.

In the following we assume an RVC period length of $t_{\text{RVC}} = 3024\,\mu\text{s}$ per cycle, each splitting its time evenly across 3 configured RSU subperiods (that is, each subperiod having a length of $t_{\text{subperiod}} = 1008\,\mu\text{s}$).

In the best case an RSU which wants to send data is already in its corresponding subperiod of the RVC period and has not used the channel for at least t_{SIFS}. Thus it takes

$$t_{\text{RSU-lower}} = t_{\text{tx-1264}} = 256\,\mu\text{s} \tag{5}$$

to transmit the frame.

In the worst case the frame does not fit into the remaining time of the ongoing subperiod of the RVC period, hence has to wait up until the next subperiod starts. Again, in the worst case, this missing time in the subperiod is just

the smallest amount of time $\epsilon = \lim_{n\to\infty} \frac{1}{n}$. Thus, the upper bound of transmit time can be calculated as

$$\begin{aligned} t_{\text{RSU-upper}} &= t_{\text{slot16}} - (t_{\text{subperiod}} - (t_{\text{SIFS}} + t_{\text{tx-1264}}) - \epsilon) \\ &\quad + t_{\text{SIFS}} + t_{\text{tx-1264}} \\ &\simeq 5968\,\mu\text{s}. \end{aligned} \tag{6}$$

Moving now to vehicles, the lower bound for transmitting data in the vehicle period is calculated as

$$t_{\text{VEH-lower}} = t_{\text{DIFS}} + 0 \times t_{\text{slot-CSMA}} + t_{\text{tx-1264}} = 314\,\mu\text{s}. \tag{7}$$

If the transmission of a vehicle fits into the vehicle period, the time to transmit a frame is uniformly distributed among the number of slots for the random waiting period (that is, CW); thus, for this case we derive a maximum transmit time of

$$\begin{aligned} t_{\text{VEH-CW-max}} &= t_{\text{DIFS}} + \text{CW} \times t_{\text{slot-CSMA}} + t_{\text{tx-1264}} \\ &= 1133\,\mu\text{s}. \end{aligned} \tag{8}$$

The upper bound of transmit time for a vehicle on an idle channel holds if the frame does not fit into the remaining time of the vehicle period and when the selected number of slots for the random waiting period is the maximum (that is, CW). This time is calculated as

$$\begin{aligned} t_{\text{VEH-upper}} &= t_{\text{RVC}} + 2 \times t_{\text{guard}} \\ &\quad + 2(t_{\text{DIFS}} + \text{CW} \times t_{\text{slot-CSMA}} + t_{\text{tx-1264}}) \\ &\quad - \epsilon \\ &\simeq 5418\,\mu\text{s}. \end{aligned} \tag{9}$$

7. Simulations

For our comparison of IEEE 802.11p and ARIB T109 we used the Open Source vehicular network simulation framework Veins [24]. It consists of two parts: OMNeT++ as a discrete event simulation kernel (the basis for its network simulation models) and SUMO [25] for modeling vehicular movement. As it already contains models that are specific to the simulation of vehicular networks (albeit with a focus on the European and U.S. family of standards), it already contains a fully functioning implementation of IEEE 802.11p (see Section 3) and is frequently used in academic research. With the parameters for the channel model having been determined (Section 5), what was left was to implement a model of the protocol layers of ARIB T109.

7.1. Model Implementation

To simulate nodes using ARIB T109 we developed a model representing the standard as OMNeT++ modules for the Veins framework. This set of modules is closely aligned with the standard; this means we include no security functions, which are out of the scope of the standard.

We distinguish between the different node types (base station and mobile station) to capture their differences in medium access (physical and virtual carrier sense functions) according to the standard. The medium access layer implementation follows the design outlined by Eckhoff et al. [26], but also includes an additional model of the *IVC-RVC Layer*, which is predominantly tasked with enforcing the TDMA scheme for accessing the channel and with handling information exchange for communication cycle configurations and time synchronization.

For realizing the physical layer we rely on the already existing and validated implementation of IEEE 802.11p in Veins, adapting parameters like carrier frequency and transmission power to match the ARIB T109 standard.

Validation of the ARIB T109 implementation followed the official test document [27]. It does not only contain test cases for the communication control and the maintenance protocol, but also technical requirements in terms of physical behavior and limits. Since the implementation of the physical layer by Eckhoff et al. [26] is commonly used in several publications and, therefore, can be assumed to be correct, we did not consider tests for the physical layer functionality. The correct functionality of the medium access layer, however, had to be validated. We focused on functionality for updating the parameters and values for the *IVC-RVC Layer* and the time synchronization. For this we used the corresponding test cases of [27] to validate our model before proceeding to the simulation study.

Figure 6: Zoomed-in rendering of the 7 km × 7 km region in the south east of Luxembourg City used for the simulative performance studies. Shown are the positions of the three RSUs (icons) as well as the 2 km × 2 km (solid outer rectangle) and the 1 km × 1 km (dashed inner rectangle) regions of data collection.

7.2. Simulation Scenario

For our simulations we chose the LuST scenario developed by Codeca et al. [28], which authors calibrated to closely model real traffic in the city of Luxembourg. The scenario provides different kinds of environments such as Luxembourg City downtown, suburbs, or highways. Furthermore, it does not only contain 24 h of vehicle mobility but also street and building information recreated in detail.

MAC	ARIB STD-T109	IEEE 802.11p
Frequency	760 MHz	5.89 GHz
Shadow fading constants	$\beta = 0.1$ dB, $\gamma = 0.4$ dB/m	$\beta = 9$ dB, $\gamma = 0.4$ dB/m
Bitrate	6 Mbit/s	6 Mbit/s
Maximum transmit power	10 dBm	20 dBm
CCA threshold	−53 dBm	−65 dBm
Sensitivity	−89 dBm	−89 dBm
AIFS (802.11p)		2 slots
CW	63 slots	3 to 7 slots
Beacon size	100 Byte	
Beacon frequency	1 Hz	
Number of RSUs	3	
Simulation time	5 s	

Table 2: Simulation parameters used for the study.

Its total area is around 156 km^2 with a total of 13 553 buildings and between 200 000 and 300 000 vehicles being simulated. During rush hour which is around 8:30h in the morning and 18:30h in the evening it simulates nearly 6000 vehicles simultaneously. We determined different regions which we used for our simulations, each representing one scenario. These regions are located in the inner city as well as in different suburban areas.

Figure 6 shows a detailed view of the scenario we focus on in this work. An average of almost 300 vehicles are driving in the center 2 km × 2 km region of a 7 km × 7 km area located in the south east of Luxembourg City. We ensured that our conclusions are equally valid for similar regions we selected. The scenario also includes three RSUs. With the exception of one study (which uses the full 7 km × 7 km scenario, but limits data collection to a 1 km × 1 km region), we report all results for data collected in this 2 km × 2 km region.

As in our analytical study, we configured an RVC period length of $t_{\mathrm{RVC}} = 3024\,\mu$s, again splitting its time evenly across 3 configured RSU subperiods, one for each RSU. Since most of the safety information being distributed will be sent by the base stations [13], we consider each of them to be of equal importance.

We also implemented a simple application layer which sends periodic broadcasts (beacons) at a rate of 1 Hz.

The complete system is then investigated for the two different communication technologies: IEEE 802.11p (we call this scenario *IEEE 802.11p*) and ARIB STD-T109 (we call this scenario *ARIB T109*). For comparison, we also simulate the scenario while disabling RSUs (we call this scenario *ARIB T109 V2V*); as this scenario allows vehicles to use the full duration of a cycle for transmitting, it allows us to differentiate the impact of physical properties from those of reduced channel capacity for vehicles.

Table 2 lists all parameters of the application layer, of the ARIB T109 and IEEE 802.11p models, and of the simulation. Note that aside from the respective parameters accurately reflecting differences in the properties of the channel and standards, the maximum transmit power has been deliberately configured to be higher for IEEE 802.11p where upper layer standards typically allow adaptive (but, overall, higher) values. Note further that, because in this study we are only interested in mean values (over a large number of samples), no fast fading model is employed.

7.3. Evaluation Metrics

As the simulation has probabilistic components we perform 60 independent repetitions with different pseudo random number generator seeds for both network simulation and road traffic models.

In order to get a holistic insight on the performance of ARIB T109 and IEEE 802.11p we chose the following metrics in the application and medium access control layer:

1. *Communication distance*: For each successfully received frame we measure the distance between receiver and sender. This is a direct indication of the effect of physical layer properties on protocol performance.
2. *Frame detection rate*: On the physical layer we measure the number of frames detected (that is, above the sensitivity threshold) per second. This metric scales with the vehicle density: a higher communication distance intuitively leads to more nodes within range, thus a higher number of detected frames per second.
3. *Channel utilization*: We periodically measure the channel utilization
$$b_t = \frac{t_{\mathrm{busy}}}{t_{\mathrm{busy}} + t_{\mathrm{idle}}} \tag{10}$$
as the fraction of the time the wireless channel was sensed busy since the last measurement of this metric. In ARIB T109 these results are recorded separately for both the RSU and vehicle period, and the measurement is performed at the end of each period. In IEEE 802.11p the measurement is performed once every 100 ms.
4. *Frame collision rate*: To be able to investigate load vs. goodput in more detail we chose the rate of collided frames as
$$p_{\mathrm{coll}} = \frac{n_{\mathrm{coll}}}{n_{\mathrm{rx}} + n_{\mathrm{coll}}}. \tag{11}$$
Here, n_{rx} denotes the number of successfully received frames, and n_{coll} denotes the number of observed frame collisions – frames which could have been decoded if there would not have been any interference on the channel. This is possible, as random processes are under control of the simulation framework, thus we can distinguish between lost frames due to interference, lost frames due to low signal strength, and lost frames due to bit errors. Note that this metric is focusing strictly on frames; higher layer protocols might potentially employ Automatic Repeat Request (ARQ) or additional Forward Error Correction (FEC) techniques to mitigate the impact of lost frames (at the price of increased utilization and delay).

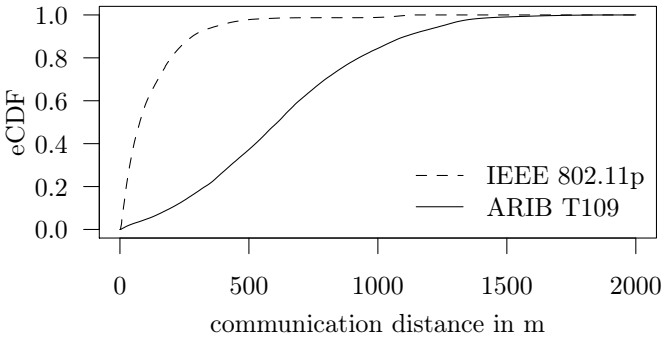

Figure 7: Communication distance of ARIB T109 in comparison to IEEE 802.11p.

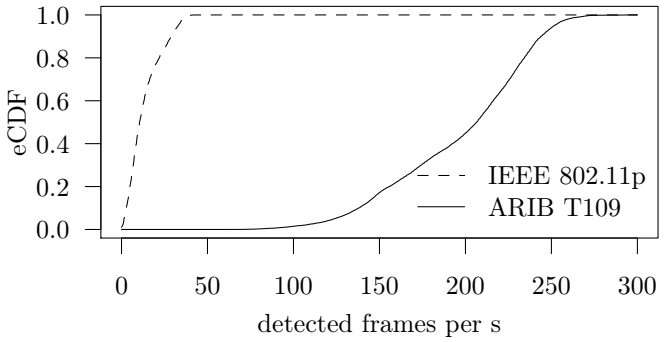

Figure 8: The total number of detected frames ARIB T109 in comparison to IEEE 802.11p.

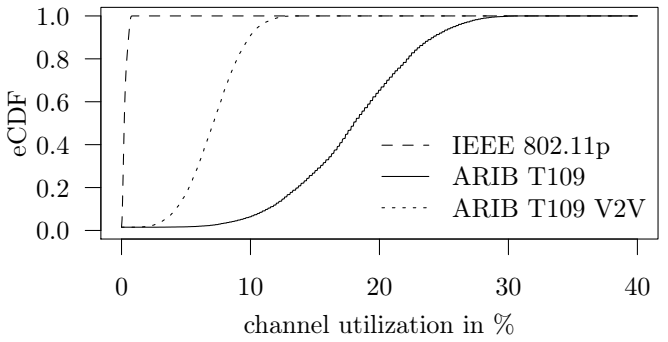

Figure 9: The MAC utilization of ARIB T109 in comparison to IEEE 802.11p.

5. *End-to-End delay*: Finally we observe the delay at the application layer. This metric mainly depends on the amount of time frames stay queued at the medium access layer plus the time needed to transmit the frame. We expect this metric to be higher in TDMA based schemes like ARIB T109 compared to pure CSMA/CA approaches like IEEE 802.11p, as frame generation processes are independent of the time slotting. Again this metric scales with the vehicle density and, thus, channel load. A higher channel busy fraction increases the probability for a failed clear channel assessment (IEEE 802.11p, and ARIB T109 in the vehicle period), thus leading to backoff. However, in TDMA approaches (ARIB T109 in the RVC period) no other node accesses the channel, thus no backoff is necessary.

8. Simulation Results

We plot simulation results for the metrics in the form of one empirical Cumulative Density Function (eCDF) each. This allows to quickly compare metrics' median (i.e., the value associated with an eCDF value of 0.5), first and third quartile (0.25 and 0.75), as well as any other quantiles.

Figure 7 shows the results of the first metric we investigated, plotting the distribution of distances at which frames were received in the IEEE 802.11p and ARIB T109 scenarios (we only plot results for the ARIB T109 scenario; the results in the ARIB T109 V2V scenario are, of course, identical). It is immediately apparent that ARIB T109 transmissions were able to reach substantially farther than IEEE 802.11p transmissions. This is in line with findings in the literature [8] and corresponds well with the theoretical limits derived in Section 6: The analytical upper limit of IEEE 802.11p transmissions in the given configuration manifests directly as the maximum of communication distance (1142 m). Yet, even though the few straight stretches of road in the scenario (which we showed in Figure 6) allowed individual IEEE 802.11p transmissions to reach these distances, most attempts at data exchange were cut short by the presence of buildings. This effect is also what keeps ARIB T109 transmissions from reaching anywhere close to their theoretical upper limit of 2800 m. Though our simulation only spans 2000 m, it is the buildings that ultimately limit the usable communication range (indeed, we retried measurements for all nodes in the full 7 km × 7 km region while measuring communication ranges in the center 1 km × 1 km region and found the theoretical upper limit of 2800 m confirmed, but no qualitatively different results). Still, because path loss and shadow fading characteristics are much more favorable, the range of ARIB T109 is substantially above that of IEEE 802.11p: The 95^{th} percentile reached as far as approximately 1250 m (as opposed to approximately 400 m for IEEE 802.11p).

Figure 8 illustrates both the positive and the negative consequence of this increased reach of ARIB T109. We plot the distribution of the number of frames detected each second at each node in the IEEE 802.11p and ARIB T109 scenarios (again, we only plot results for the ARIB T109 scenario; the results in the ARIB T109 V2V scenario are comparable as the added load by RSUs is negligible). It is evident that the median number of detected frames per second is more than tenfold increased in the ARIB scenario. While this has obvious benefits, e.g., for safety applications it is indicative of a much more crowded channel. It is well known that a CSMA/CA access scheme becomes increasingly inefficient as the channel gets more saturated [29]; therefore, ARIB T109 (following its philosophy that RSUs are the more important participants) addresses this problem via its TDMA mechanism.

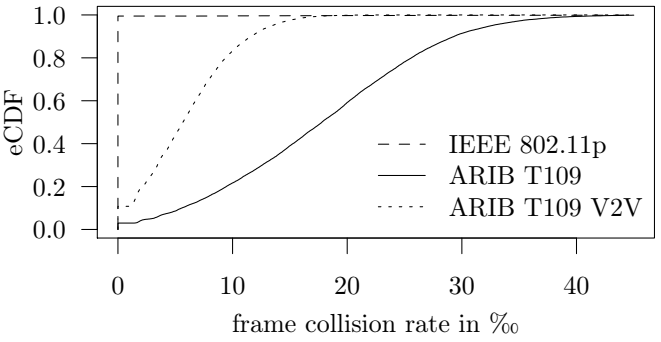

Figure 10: The frame collision rate of frames sent by RSUs and vehicles in ARIB T109 in comparison to IEEE 802.11p.

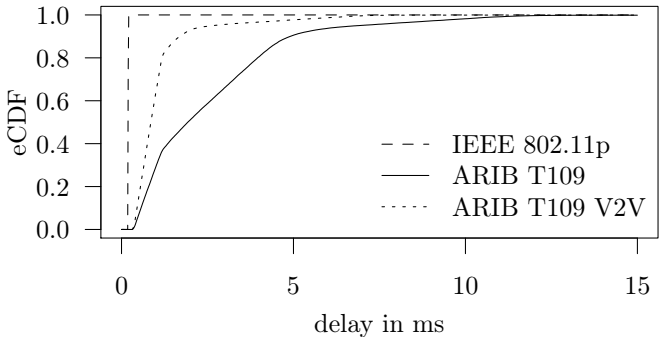

Figure 11: The delay of ARIB T109 in comparison to IEEE 802.11p.

Figure 9 reveals the consequences of this decision. Here we compare the channel utilization of the IEEE 802.11p scenario with that of ARIB T109. If RSUs are disabled (*ARIB T109 V2V* scenario), the better reach of ARIB T109 already results in a channel utilization with a more than tenfold higher median – a clear drawback of the higher reach. Considering the envisioned use case of ARIB T109, that is, looking at the *ARIB T109* scenario, allows us to paint a more differentiated picture, though: Because RSUs can coordinate channel access in exclusive slots they do not suffer from increased channel utilization or interference (this data therefore not being included in the graph). On the negative side, the now reduced channel capacity for vehicles causes their perceived channel utilization to climb to approximately three times higher values.

Figure 10 demonstrates the impact this has on frame collisions. While no frames sent by RSUs are lost to collisions in ARIB T109 (data not shown), owing to each RSU having a reserved subperiod, the downside of the TDMA scheme of ARIB T109 manifests quite plainly for vehicles, as these now suffer doubly (from more received traffic on a channel of less capacity). While frame collisions are at negligible values for IEEE 802.11p transmissions, ARIB T109 transmissions suffer from noticeably increased frame collision rates during periods of time allotted to vehicles. Still, with values of only a few in every thousand frames being lost to collisions, both ARIB T109 and IEEE 802.11p can be seen to work within acceptable parameters. Instead, the difference lies in the last metric we will investigate.

Figure 11 illustrates that, for all its benefits for RSUs, the application of TDMA brings with it an increase in application layer message delay. In IEEE 802.11p, transmissions can be sent almost instantly (we record a median below 0.2 ms). In the ARIB T109 V2V scenario the overall larger CW already takes delays up into the 1 ms range (corresponding to the value derived in equation 8) with the increased channel load causing spikes in delay into the upper single digit range. With the addition of RSUs in the ARIB T109 scenario, the TDMA scheme is in effect. Transmissions cannot be sent at arbitrary times, but routinely need to be delayed until they fit into the next available time slot, yielding a base delay of up to approximately 5 ms (corresponding to the value derived in equation 9). This base delay is further compounded by the reduced channel capacity for vehicles, resulting in additional queueing delays. Still, the total delay in the ARIB T109 scenario stays below 7 ms for 95 % of transmissions, below 11 ms for 99 % of transmissions.

9. Conclusion

In this work we presented a first performance comparison of the two very different standards for vehicular communication IEEE 802.11p and ARIB T109 that respects not just their differences in terms of physical layer (5.9 GHz vs. 700 MHz band), but also their very different medium access characteristics: While IEEE 802.11p uses pure CSMA/CA to coordinate multiple access among different vehicles, ARIB T109 uses TDMA to reserve time slots for exclusive use by Roadside Units (RSUs).

We based this comparison on our new Open Source implementation of the ARIB T109 standard for the vehicular network simulation framework Veins, validating results against analytics. The model also encompasses parameters for a computationally inexpensive shadow fading model for suburban environments. We briefly reported on the results of an extensive measurement campaign that underlies these parameters.

Our performance comparison demonstrates that, in suburban environments, ARIB T109 transmissions reach much farther as they suffer much less from obstacle shadowing by buildings, backing up earlier results. This can benefit safety applications in Non Line of Sight (NLOS) conditions as well as multi-hop information, e.g., for traffic efficiency applications. When investigating higher layer performance, however, this characteristic also leads to increased load and increased interference on the channel. Moving still higher in the protocol stack, it can be seen that the TDMA mechanism of ARIB T109 can compensate the negative impact of this effect by allocating dedicated transmissions for RSUs guaranteeing ideal channel conditions for them. The flip side of this are somewhat increased delays and even further reduced channel capacity (and, thus, increased frame loss due to collisions) for vehicles.

Acknowledgements

The authors would like to thank M. Nabeel, B. Bloessl, J. Blobel, and D. S. Buse for their support during the measurement campaign.

References

[1] J. Harding, G. Powell, R. Yoon, J. Fikentscher, C. Doyle, D. Sade, M. Lukuc, J. Simons, J. Wang, Vehicle-to-Vehicle Communications: Readiness of V2V Technology for Application, NHTSA Technical Report DOT HS 812 014, National Highway Traffic Safety Administration (Aug. 2014).

[2] C. Sommer, F. Dressler, Vehicular Networking, Cambridge University Press, 2014. doi:10.1017/CBO9781107110649.

[3] IEEE, Wireless Access in Vehicular Environments, Std 802.11p-2010, IEEE (Jul. 2010). doi:10.1109/IEEESTD.2010.5514475.

[4] ARIB, 700 MHz Band Intelligent Transport Systems, STD T109-v1.2, ARIB (Dec. 2013).

[5] C. Sommer, R. German, F. Dressler, Bidirectionally Coupled Network and Road Traffic Simulation for Improved IVC Analysis, IEEE Transactions on Mobile Computing 10 (1) (2011) 3–15. doi:10.1109/TMC.2010.133.

[6] J. Heinovski, F. Klingler, F. Dressler, C. Sommer, Performance Comparison of IEEE 802.11p and ARIB STD-T109, in: 8th IEEE Vehicular Networking Conference (VNC 2016), IEEE, Columbus, OH, 2016, pp. 1–8. doi:10.1109/VNC.2016.7835923.

[7] R. Sevlian, C. Chun, I. Tan, A. Bahai, K. Laberteaux, Channel Characterization for 700 MHz DSRC Vehicular Communication, Journal of Electrical and Computer Engineering 2010. doi:10.1155/2010/840895.

[8] H. Fernandez, L. Rubio, V. M. Rodrigo-Penarrocha, J. Reig, Path Loss Characterization for Vehicular Communications at 700 MHz and 5.9 GHz Under LOS and NLOS Conditions, IEEE Antennas and Wireless Propagation Letters 13 (2014) 931–934. doi:10.1109/lawp.2014.2322261.

[9] L. Rubio, H. Fernández, V. M. Rodrigo-Peñarrocha, J. Reig, Path loss characterization for vehicular-to-infrastructure communications at 700 MHz and 5.9 GHz in urban environments, in: 2015 IEEE International Symposium on Antennas and Propagation & USNC/URSI National Radio Science Meeting, IEEE, Vancouver, Canada, 2015, pp. 93–94. doi:10.1109/APS.2015.7304432.

[10] L. Rubio, V. M. Rodrigo-Penarrocha, J. Reig, H. Fernandez, Investigation of the path loss propagation for V2V communications in the opposite direction, in: IEEE International Symposium on Antennas and Propagation (APS/URSI 2016), IEEE, Fajardo, Puerto Rico, 2016, pp. 1685–1686. doi:10.1109/aps.2016.7696549.

[11] K. Minato, H. Cheng, Y. Yamao, Performance of broadcast transmission from multiple vehicles in vehicle-roadside-vehicle relay network, in: 6th International ICST Conference on Communications and Networking in China (CHINACOM 2011), IEEE, Harbin, 2011, pp. 675–679. doi:10.1109/ChinaCom.2011.6158240.

[12] ITU-R, Propagation data and prediction methods for the planning of short-range outdoor radiocommunication systems and radio local area networks in the frequency range 300 MHz to 100 GHz, Recommendation P.1411-1, International Telecommunications Union (2001).

[13] S. Sai, T. Oshida, R. Onishi, A. Yoshioka, H. Tanaka, Comparisons of Non-Line-Of-Sight Inter-Vehicle Communications in the Urban Environment Between 5.9GHz and 700MHz Bands, in: 4th IEEE Vehicular Networking Conference (VNC 2012), Poster Session, IEEE, Seoul, Korea, 2012, pp. 144–151.

[14] ITU-R, Propagation data and prediction methods for the planning of short-range outdoor radiocommunication systems and radio local area networks in the frequency range 300 MHz to 100 GHz, Recommendation P.1411-6, International Telecommunications Union (2012).

[15] A. Abunei, C.-R. Comsa, I. Bogdan, RSS improvement in VANETs by auxilliary transmission at 700 MHz, in: International Symposium on Signals, Circuits and Systems (ISSCS 2015), IEEE, Iasi, Romania, 2015. doi:10.1109/isscs.2015.7203998.

[16] C. Sommer, D. Eckhoff, R. German, F. Dressler, A Computationally Inexpensive Empirical Model of IEEE 802.11p Radio Shadowing in Urban Environments, in: 8th IEEE/IFIP Conference on Wireless On demand Network Systems and Services (WONS 2011), IEEE, Bardonecchia, Italy, 2011, pp. 84–90. doi:10.1109/WONS.2011.5720204.

[17] T. Yokomori, M. Fujii, H. Hatano, A. Ito, Y. Watanabe, A comparative study on access control methods for ITS radio communications systems, in: 4th IEEE Global Conference on Consumer Electronics (GCCE 2015), IEEE, Osaka, Japan, 2015, pp. 155–158. doi:10.1109/gcce.2015.7398598.

[18] T. Yokomori, M. Fujii, H. Hatano, A. Ito, Y. Watanabe, An improvement of media access control scheme for inter-vehicle communications, in: International Symposium on Information Theory and Its Applications (ISITA 2016), IEEE, Monterey, CA, 2016, pp. 360–364.

[19] Wireless LAN Medium Access Control (MAC) and Physical Layer (PHY) specifications, Std 802.11a-1999, IEEE (1999).

[20] IEEE, IEEE Guide for Wireless Access in Vehicular Environments (WAVE) - Architecture, Std 1609.0-2013, IEEE (Mar. 2014). doi:10.1109/IEEESTD.2014.6755433.

[21] European Telecommunications Standards Institute, Intelligent Transport Systems (ITS); European profile standard for the physical and medium access control layer of Intelligent Transport Systems operating in the 5 GHz frequency band, ES 202 663 V1.1.0, ETSI (Nov. 2009).

[22] H. Friis, A Note on a Simple Transmission Formula, Proceedings of the IRE 34 (5) (1946) 254–256. doi:10.1109/JRPROC.1946.234568.

[23] IEEE, Wireless LAN Medium Access Control (MAC) and Physical Layer (PHY) Specifications, Std 802.11-2012, IEEE (2012).

[24] C. Sommer, Z. Yao, R. German, F. Dressler, Simulating the Influence of IVC on Road Traffic using Bidirectionally Coupled Simulators, in: 27th IEEE Conference on Computer Communications (INFOCOM 2008): IEEE Workshop on Mobile Networking for Vehicular Environments (MOVE 2008), IEEE, Phoenix, AZ, 2008, pp. 1–6. doi:10.1109/INFOCOM.2008.4544655.

[25] D. Krajzewicz, G. Hertkorn, C. Rössel, P. Wagner, SUMO (Simulation of Urban MObility); An Open-source Traffic Simulation, in: 4th Middle East Symposium on Simulation and Modelling (MESM 2002), Sharjah, United Arab Emirates, 2002, pp. 183–187.

[26] D. Eckhoff, C. Sommer, F. Dressler, On the Necessity of Accurate IEEE 802.11p Models for IVC Protocol Simulation, in: 75th IEEE Vehicular Technology Conference (VTC2012-Spring), IEEE, Yokohama, Japan, 2012, pp. 1–5. doi:10.1109/VETECS.2012.6240064.

[27] ARIB, 700 MHz Band Intelligent Transport Systems Test Items And Conditions For Mobile Station Compatibility Confirmation, TR T20-v1.1, ARIB (Dec. 2012).

[28] L. Codeca, R. Frank, T. Engel, Luxembourg SUMO Traffic (LuST) Scenario: 24 Hours of Mobility for Vehicular Networking Research, in: 7th IEEE Vehicular Networking Conference (VNC 2015), IEEE, Kyoto, Japan, 2015. doi:10.1109/VNC.2015.7385539.

[29] Y. P. Fallah, C.-L. Huang, R. Sengupta, H. Krishnan, Analysis of Information Dissemination in Vehicular Ad-Hoc Networks With Application to Cooperative Vehicle Safety Systems, IEEE Transactions on Vehicular Technology 60 (1) (2011) 233–247. doi:10.1109/tvt.2010.2085022.